

Bronchial				Nasal				Q	Q P value	Reference
$\beta$	SD	P value	FDR	$\beta$	SD	P value	FDR			
-0.306	0.040	$3.101 \times 10^{-10}$	$1.907 \times 10^{-06}$	-0.506	0.049	$7.303 \times 10^{-14}$	$1.365 \times 10^{-09}$	9.998	$1.568 \times 10^{-03}$	4
<b>0.168</b>	<b>0.025</b>	<b><math>1.068 \times 10^{-08}</math></b>	<b><math>3.841 \times 10^{-05}</math></b>	<b>-0.010</b>	<b>0.044</b>	<b><math>8.137 \times 10^{-01}</math></b>	<b><math>9.638 \times 10^{-01}</math></b>	<b>12.372</b>	<b><math>4.359 \times 10^{-04}</math></b>	5
<b>-0.188</b>	<b>0.031</b>	<b><math>1.190 \times 10^{-07}</math></b>	<b><math>2.872 \times 10^{-04}</math></b>	<b>-0.022</b>	<b>0.033</b>	<b><math>5.043 \times 10^{-01}</math></b>	<b><math>9.454 \times 10^{-01}</math></b>	<b>13.442</b>	<b><math>2.461 \times 10^{-04}</math></b>	6
0.104	0.018	$2.326 \times 10^{-07}$	$5.116 \times 10^{-04}$	0.046	0.019	$1.660 \times 10^{-02}$	$6.814 \times 10^{-01}$	4.911	$2.669 \times 10^{-02}$	5
1.456	0.254	$4.908 \times 10^{-07}$	$9.623 \times 10^{-04}$	1.206	0.249	$1.229 \times 10^{-05}$	$1.516 \times 10^{-02}$	0.494	$4.821 \times 10^{-01}$	7
0.368	0.070	$2.522 \times 10^{-06}$	$3.756 \times 10^{-03}$	0.272	0.080	$1.286 \times 10^{-03}$	$3.134 \times 10^{-01}$	0.816	$3.665 \times 10^{-01}$	8
<b>0.130</b>	<b>0.027</b>	<b><math>1.123 \times 10^{-05}</math></b>	<b><math>1.264 \times 10^{-02}</math></b>	<b>0.031</b>	<b>0.023</b>	<b><math>1.752 \times 10^{-01}</math></b>	<b><math>8.909 \times 10^{-01}</math></b>	<b>7.791</b>	<b><math>5.251 \times 10^{-03}</math></b>	6
<b>0.161</b>	<b>0.035</b>	<b><math>2.191 \times 10^{-05}</math></b>	<b><math>2.135 \times 10^{-02}</math></b>	<b>0.047</b>	<b>0.026</b>	<b><math>7.880 \times 10^{-02}</math></b>	<b><math>8.350 \times 10^{-01}</math></b>	<b>6.836</b>	<b><math>8.932 \times 10^{-03}</math></b>	6
-0.584	0.130	$3.757 \times 10^{-05}$	$3.245 \times 10^{-02}$	-0.658	0.134	$9.638 \times 10^{-06}$	$1.260 \times 10^{-02}$	0.157	$6.918 \times 10^{-01}$	7
0.289	0.065	$4.097 \times 10^{-05}$	$3.452 \times 10^{-02}$	0.201	0.061	$1.780 \times 10^{-03}$	$3.591 \times 10^{-01}$	0.975	$3.235 \times 10^{-01}$	5
0.193	0.044	$5.459 \times 10^{-05}$	$4.266 \times 10^{-02}$	0.267	0.044	$1.466 \times 10^{-07}$	$4.029 \times 10^{-04}$	1.414	$2.344 \times 10^{-01}$	6
-0.220	0.053	$1.263 \times 10^{-04}$	$7.709 \times 10^{-02}$	-0.530	0.078	$1.146 \times 10^{-08}$	$4.877 \times 10^{-05}$	10.806	$1.012 \times 10^{-03}$	6
-0.303	0.074	$1.601 \times 10^{-04}$	$9.022 \times 10^{-02}$	-0.381	0.084	$3.782 \times 10^{-05}$	$3.544 \times 10^{-02}$	0.485	$4.860 \times 10^{-01}$	9
0.149	0.040	$4.407 \times 10^{-04}$	$1.694 \times 10^{-01}$	0.380	0.075	$5.672 \times 10^{-06}$	$8.341 \times 10^{-03}$	7.386	$6.575 \times 10^{-03}$	7
0.153	0.051	$4.047 \times 10^{-03}$	$4.650 \times 10^{-01}$	0.322	0.055	$4.100 \times 10^{-07}$	$9.483 \times 10^{-04}$	5.077	$2.425 \times 10^{-02}$	7
-0.079	0.027	$5.265 \times 10^{-03}$	$5.049 \times 10^{-01}$	-0.133	0.022	$2.423 \times 10^{-07}$	$6.148 \times 10^{-04}$	2.404	$1.210 \times 10^{-01}$	6

provide a comprehensive catalog of the bronchial nasal eQTLs in this article's Online Repository at [www.jacionline.org](http://www.jacionline.org), which can be queried for future studies. We conclude that the usability of nasal brushings as a marker of the bronchial epithelial gene expression and eQTLs to find noncoding risk variants can be a promising experimental approach; however, it is highly gene-dependent.

Kai Imkamp, MD<sup>a,b</sup>  
Marijn Berg<sup>a,b,c</sup>  
Cornelis J. Vermeulen, PhD<sup>a,b</sup>  
Irene H. Heijink, PhD<sup>b,c</sup>  
Victor Guryev, PhD<sup>b,d</sup>  
Huib A. M. Kerstjens, MD, PhD<sup>a,b</sup>  
Gerard H. Koppelman, MD, PhD<sup>b,e</sup>  
Maarten van den Berge, MD, PhD<sup>a,b,\*</sup>  
Alen Faiz, PhD<sup>a,b,c,\*</sup>

From <sup>a</sup>the Department of Pulmonology, University Medical Center Groningen, <sup>b</sup>GRiAC (Groningen Research Institute for Asthma and COPD), Beatrix Children's Hospital, University Medical Center Groningen, <sup>c</sup>the Department of Pathology & Medical Biology, Section of Medical Biology, University Medical Center Groningen, <sup>d</sup>the European Research Institute for the Biology of Ageing, University Medical Center Groningen, and <sup>e</sup>the Department of Pediatric Pulmonology and Pediatric Allergology, Beatrix Children's Hospital, University Medical Center Groningen, Groningen, The Netherlands. E-mail: [k.inkamp@umcg.nl](mailto:k.inkamp@umcg.nl).

\*Joint last authors.

A.F. was funded by a Junior Investigator Longfonds grant (4.2.16.132JO) and a Stichting Astma Bestrijding grant.

Disclosure of potential conflict of interest: C. J. Vermeulen reports institutional grants pending from GlaxoSmithKline. H. A. M. Kerstjens reports institutional grants from Novartis, Boehringer Ingelheim, and GSK; speaking fees from Boehringer Ingelheim; consultant fees from AstraZeneca, Chiesi, GlaxoSmithKline, and Novartis; board membership with Chiesi, GlaxoSmithKline, and Novartis; and institutional patient fees collected during the course of the trial. G. H. Koppelman reports institutional grants from the Lung Foundation of the Netherlands, TEVA, GlaxoSmithKline, Ubbo Emmius Foundation, and TETRI Foundation. M. van den Berge reports institutional grants pending from Chiesi, GlaxoSmithKline, and TEVA. The rest of the authors declare that they have no relevant conflicts of interest.

## REFERENCES

- Sridhar S, Schembri F, Zeskind J, Shah V, Gustafson AM, Steiling K, et al. Smoking-induced gene expression changes in the bronchial airway are reflected in nasal and buccal epithelium. *BMC Genomics* 2008;9:259.
- Zhang X, Sebastiani P, Liu G, Schembri F, Zhang X, Dumas YM, et al. Similarities and differences between smoking-related gene expression in nasal and bronchial epithelium. *Physiol Genomics* 2010;41:1-8.

- Poole A, Urbanek C, Eng C, Schageman J, Jacobson S, O'connor BP, et al. Dissecting childhood asthma with nasal transcriptomics distinguishes subphenotypes of disease. *J Allergy Clin Immunol* 2014;133:670-8.e12.
- Bønnelykke K, Sleiman P, Nielsen K, Kreiner-Møller E, Mercader JM, Belgrave D, et al. A genome-wide association study identifies CDHR3 as a susceptibility locus for early childhood asthma with severe exacerbations. *Nat Genet* 2014;46:51-5.
- Hobbs BD, De Jong K, Lamontagne M, Bossé Y, Shrine N, Artigas MS, et al. Genetic loci associated with chronic obstructive pulmonary disease overlap with loci for lung function and pulmonary fibrosis. *Nat Genet* 2017;49:426-32.
- Wain LV, Shrine N, Artigas MS, Erzurumluoglu AM, Noyvert B, Bossini-Castillo L, et al. Genome-wide association analyses for lung function and chronic obstructive pulmonary disease identify new loci and potential druggable targets. *Nat Genet* 2017;49:416-25.
- Hirota T, Takahashi A, Kubo M, Tsunoda T, Tomita K, Doi S, et al. Genome-wide association study identifies three new susceptibility loci for adult asthma in the Japanese population. *Nat Genet* 2011;43:893-6.
- Torgerson DG, Ampleford EJ, Chiu GY, Gauderman WJ, Gignoux CR, Graves PE, et al. Meta-analysis of genome-wide association studies of asthma in ethnically diverse North American populations. *Nat Genet* 2011;43:887-92.
- Noguchi E, Sakamoto H, Hirota T, Ochiai K, Imoto Y, Sakashita M, et al. Genome-wide association study identifies HLA-DP as a susceptibility gene for pediatric asthma in Asian populations. *PLoS Genet* 2011;7:e1002170.

Available online March 6, 2018.  
<https://doi.org/10.1016/j.jaci.2018.01.047>

## A RAB27A 5' untranslated region structural variant associated with late-onset hemophagocytic lymphohistiocytosis and normal pigmentation



To the Editor:

Autosomal-recessive mutations in genes required for secretory lysosome-mediated lymphocyte cytotoxicity cause primary hemophagocytic lymphohistiocytosis (HLH), an early-onset, life-threatening hyperinflammatory syndrome.<sup>1</sup> Similarly, mutations in RAB27A and LYST are associated with HLH, yet manifest hypopigmentation, because Rab27a and LYST also facilitate trafficking of pigment-containing lysosomes in melanocytes.<sup>2</sup> We detail individuals from 5 families from the Baltic

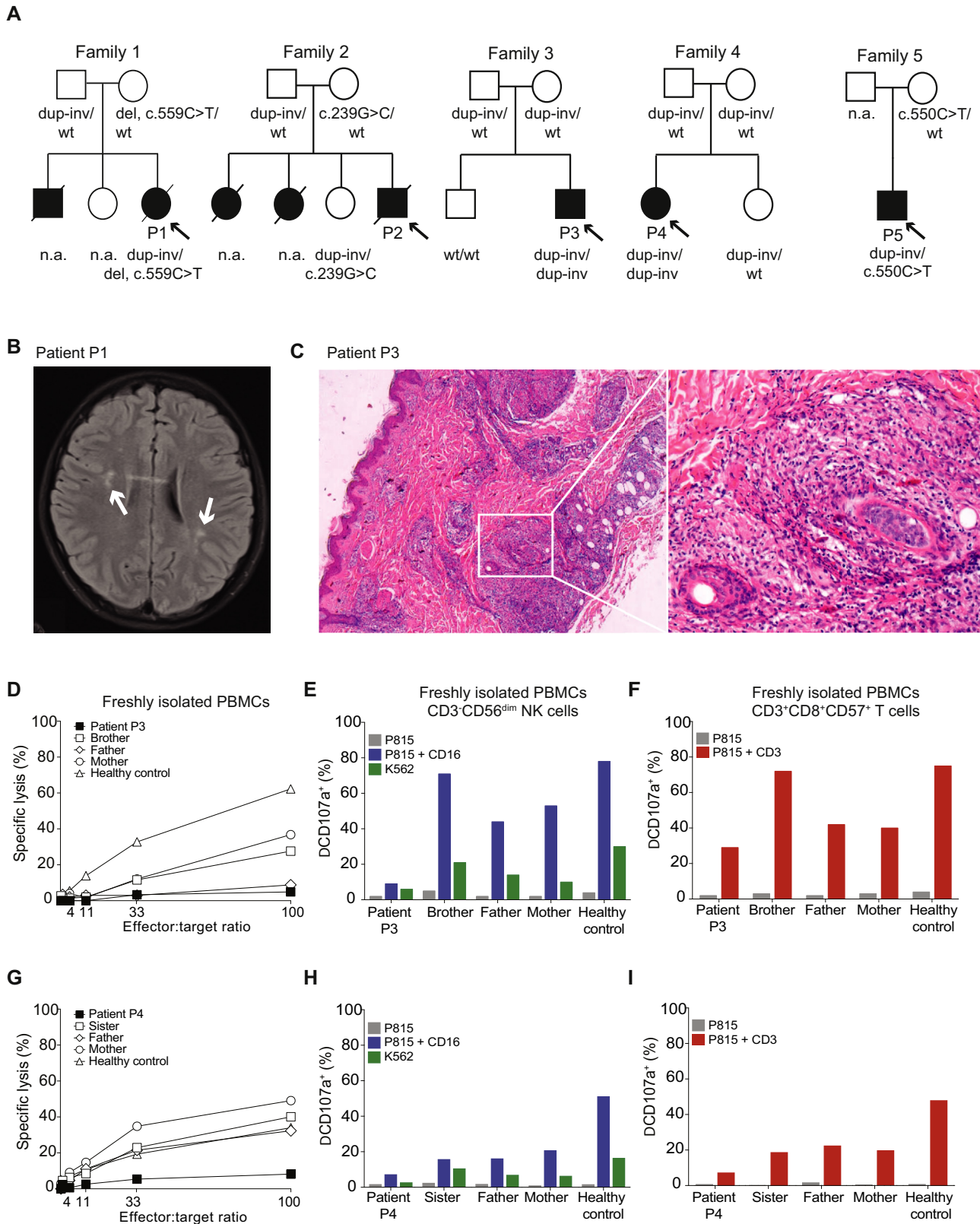


**FIG 1.** Clinical and laboratory findings. **A**, Family pedigrees and *RAB27A* genotype. **B**, Brain axial magnetic resonance imaging FLAIR images of P1 at diagnosis of HLH showed nonspecific multifocal hyperintense white matter lesions (arrows). **C**, H&E stain of a skin biopsy from P3 reveals granulomatous infiltrates in the dermis. A nonnecrotizing granuloma (boxed area, left) is presented at a higher magnification (right). **D**, NK-cell cytotoxic activity of P3 was defective compared with relatives and controls. NK-cell exocytosis (**E**) and T-cell exocytosis (**F**) were reduced in P3. NK-cell cytotoxicity (**G**) and NK (**H**) and T-cell exocytosis (**I**) were defective in P4. *dup-inv*, Duplication/inversion; *H&E*, hematoxylin and eosin; *n.a.*, not applicable/available; *wt*, wild type.

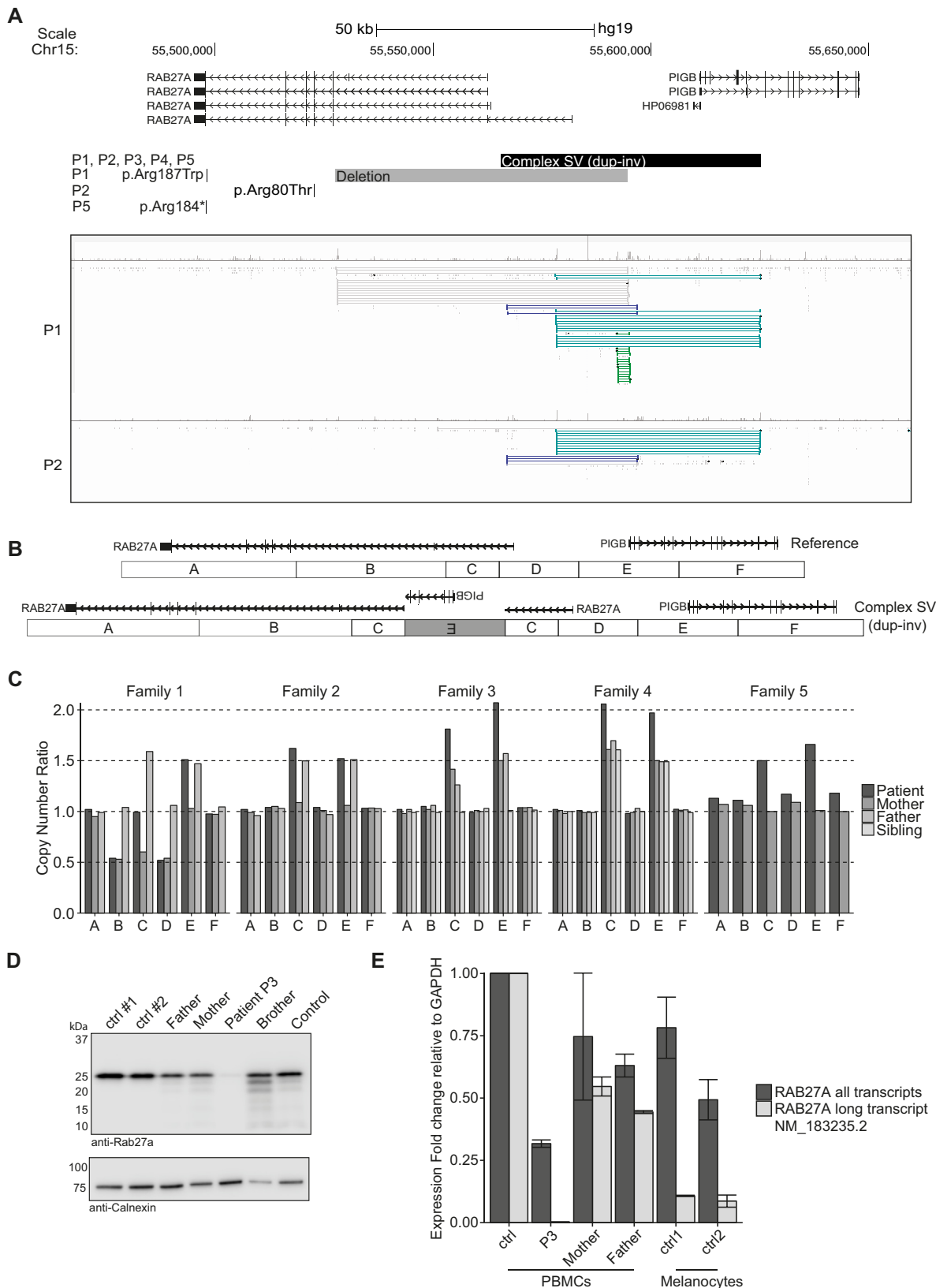


**FIG 2.** Genetic findings. **A**, Genome browser view over the region chr15:55,467,465-55,656,511 (hg19) including *RAB27A* and *PIGB* genes, with screenshots for P1 and P2 showing discordant read pairs. **B**, Model for the complex SV. **C**, Segregation analysis by MLPA. **D**, Rab27a expression in PBMcs evaluated by Western blot in P3, relatives, and healthy controls. **E**, mRNA expression of *RAB27A* in PBMcs and melanocytes. The expression of the transcript NM\_183235.2 (long) was compared with the total expression of *RAB27A*. *dup-inv*, Duplication/inversion; *GAPDH*, glyceraldehyde 3-phosphate dehydrogenase.

area with a novel structural variant at the 5' untranslated region (UTR) of *RAB27A* associated with an atypical form of Griscelli syndrome type 2 (GS2) manifesting as late-onset HLH, marked neuroinflammation, skin granulomas, lymphoma, and normal pigmentation (see Table E1 in this article's Online Repository at [www.jacionline.org](http://www.jacionline.org)).

In brief, patient 1 (P1) developed HLH at age 13 years after 8 years of recurrent neuroinflammation (Fig 1, A and B; see Fig E1, A, in this article's Online Repository at [www.jacionline.org](http://www.jacionline.org)). Her older brother died in infancy because of severe infectious mononucleosis. Patient 2 (P2) developed fatal HLH at age 15 years. Two of his 3 sisters died at age 13 years, one of an HLH-like syndrome and the other because of brain lymphoma. Patient 3 (P3) developed HLH at age 9 years, after 3 years of recurrent neuroinflammation (Fig E1, B). Patient 4 (P4) suffered from isolated neuroinflammation, without fulfilling HLH criteria. P2, P3, and P4 also had skin granulomas (Fig 1, C). Patient 5 (P5) suffered from recurrent fever flares and EBV viremia, and developed lymphoma at age 13 years. Hypopigmentation was not evident in any of the patients (Fig E1, D). Further clinical information and methods are provided in this article's Online Repository at [www.jacionline.org](http://www.jacionline.org).

Prompted by a suspicion of HLH, functional investigations of cytotoxic lymphocytes were performed on P1, P3, P4, and P5 (Table E1). Natural killer (NK)-cell cytotoxicity was defective (Fig 1, D and G). Moreover, NK- and T-cell exocytosis was impaired (Fig 1, E and F, H and I), with IL-2 stimulation inducing a partial recovery (see Fig E2, A-F, in this article's Online Repository at [www.jacionline.org](http://www.jacionline.org)). Results therefore indicated primary HLH due to defective exocytosis.

Despite the clinical and immunological findings, a molecular diagnosis of primary HLH was not established by exome sequencing of HLH-associated genes. A heterozygous *RAB27A* missense variant of unknown significance (p.Arg187Trp) was identified in P1. Moreover, previously reported heterozygous *RAB27A* mutations were detected in P2 (p.Arg80Thr) and P5 (p.Arg184\*) (Fig 2, A).<sup>3</sup> To identify possible noncoding mutations, we performed whole-genome sequencing of P1 and P2. Inspection of sequencing data revealed several read pairs aberrant for insert size and orientation at the 5'UTR of *RAB27A* and over the first 5 exons of the adjacent *PIGB*, required for glycosylphosphatidylinositol anchor biosynthesis (Fig 2, A). Software-based analysis of structural variants (SVs) confirmed the presence of multiple overlapping SVs in this region, including shared events between P1 and P2 (Fig 2, A).

To confirm the presence of SVs affecting copy number at the 5'UTR of *RAB27A*, a custom multiplex ligation-dependent probe amplification (MLPA) assay was designed. In P1, a complex SV with a duplication-normal-duplication pattern inherited from the father was confirmed, in addition to a 65-kb deletion inherited from the mother (Fig 2, A and C). P2 and P5, who carried monoallelic coding mutations, were heterozygous for the complex SV (Fig 2, C). Complex SVs are usually associated with cryptic rearrangements.<sup>4</sup> Further analysis of split reads and discordant read pairs of the complex SV indicated that one of the duplicated regions was inverted (Fig 2, B and C). In this model, only 1 of several transcriptional start sites (TSSs) of *RAB27A*, encoding the transcript NM\_183235.2, is disrupted by the complex SV, while a copy of *PIGB* remains intact (Fig 2, B). Validation of one predicted breakpoint supported this model

(see Fig E3, A, in this article's Online Repository at [www.jacionline.org](http://www.jacionline.org)). Together, identification of biallelic mutations in *RAB27A* established a diagnosis of atypical GS2 in P1, P2, and P5.

The clinical resemblance and geographic proximity prompted analysis of *RAB27A* by MLPA in P3 and P4, patients who displayed defective lymphocyte exocytosis yet lacked a genetic diagnosis. Indeed, MLPA revealed homozygosity for the complex SV in both patients (Fig 2, C), as confirmed through sequencing of a breakpoint (Fig E3, A). Rab27a protein expression was absent in leukocytes from P3, P4, and P5 (Fig 2, D, and Fig E2, G and H). Thus, all 5 patients carried biallelic *RAB27A* mutations, and were at least heterozygous for the SV affecting the transcript NM\_183235.2.

Eight patients with GS2 and normal pigmentation have been reported to date, all with missense mutations that selectively disrupt binding of Rab27a to Munc13-4 but not to melanophilin, explaining defective lymphocyte yet normal melanocyte function.<sup>5,6</sup> Because the complex SV disrupts only 1 of several TSSs of *RAB27A*, we hypothesized that lymphocytes and melanocytes might selectively use distinct *RAB27A* TSSs. Quantitative PCR demonstrated diminished expression of transcript NM\_183235.2 in peripheral blood leukocytes from P3 (Fig 2, E), suggesting predominant usage of the TSS for this transcript. This observation is also supported by cap analysis gene expression data from the FANTOM5 project (Fig E3, C-E).<sup>7</sup> In contrast, primary as well as embryonic stem cell-derived melanocytes use alternative, downstream TSSs, which were not disrupted by the complex SV (Fig E3, D and E). Quantitative PCR in primary melanocytes confirmed a smaller contribution of transcript NM\_183235.2 to total *RAB27A* expression (Fig 2, E). Transcription of *PIGB* was maintained by the complex SV (Fig E3, B). Notably, an individual with a homozygous deletion encompassing all *RAB27A* TSSs displayed classic silvery hair.<sup>8</sup> Our data therefore indicate differential TSS usage between leukocytes and melanocytes, explaining the normal pigmentation observed in patients with at least 1 mutation affecting only the upstream *RAB27A* TSS.

Nonsense mutations in *RAB27A* are associated with the development of HLH within the first year of life.<sup>3</sup> Neurologic involvement affects 55% of patients at diagnosis and 67% during the course of disease.<sup>3</sup> Three of the 5 patients reported here displayed severe and recurrent neuroinflammation resembling acute disseminated encephalomyelitis, which preceded onset of full-blown HLH by many years. Functional assays of NK- and T-cell exocytosis should therefore be considered in the diagnostic workup of patients with unexplained neuroinflammatory diseases. Late-onset HLH suggests downstream transcription in activated lymphocytes.

In conclusion, we report 5 patients with atypical GS2 characterized by neuroinflammation, lymphoma, and late-onset HLH. Remarkably, 3 patients manifested skin granulomas.<sup>9</sup> Our results elucidate novel structural aberrations affecting the noncoding region of *RAB27A*, linking the lack of hypopigmentation to differential *RAB27A* TSS usage between lymphocytes and melanocytes. The identification of a recurrent complex SV in *RAB27A* suggests a founder effect in the Baltic population. Assessment of this aberration should be included in the genetic workup of patients with defective exocytosis from this area.

We thank all family members for their participation. We also thank Stanley Sing Hoi Cheuk for providing melanocytes, the Department of Clinical Genetics of the Karolinska University Hospital for help with MLPA, and the Clinical Genomics unit at SciLifeLab for whole-genome sequencing.

Bianca Tesi, MD, PhD<sup>a,b</sup>  
 Jelena Rascon, MD, PhD<sup>c,d</sup>  
 Samuel C. C. Chiang, PhD<sup>e,\*</sup>  
 Birute Burnyte, PhD<sup>f</sup>  
 Alexandra Löfstedt, MD<sup>a,b</sup>  
 Anders Fasth, MD, PhD<sup>g</sup>  
 Miriam Heizmann, Mbiol<sup>h,i</sup>  
 Sandra Juozapaite, MD<sup>j</sup>  
 Rosita Kiudeliene, MD<sup>j</sup>  
 Egle Kvedaraitė, MD<sup>o</sup>  
 Valdona Miseviciene, MD<sup>k</sup>  
 Audrone Muleviciene, MD<sup>c,d</sup>  
 Martha-Lena Müller, PhD<sup>e,\*</sup>  
 Magnus Nordenskjöld, MD, PhD<sup>b</sup>  
 Reda Matuzeviciene, MD, PhD<sup>l,m</sup>  
 Ruta Samaitiene, MD, PhD<sup>l,n</sup>  
 Carsten Speckmann, MD<sup>b</sup>  
 Sigit Stankeviciene, MD<sup>c</sup>  
 Vytautas Zekas, MD<sup>d</sup>  
 Matthias Voss, PhD<sup>e</sup>  
 Stephan Ehl, MD, PhD<sup>h</sup>  
 Nerija Vaiciene-Magistris, MD, PhD<sup>o</sup>  
 Jan-Inge Henter, MD, PhD<sup>a</sup>  
 Marie Meeths, MD, PhD<sup>a,b,†</sup>  
 Yen-an T. Bryceson, PhD<sup>e,p,†</sup>

From <sup>a</sup>the Childhood Cancer Research Unit, Department of Women's and Children's Health, Karolinska Institutet, Karolinska University Hospital Solna and <sup>b</sup>the Clinical Genetics Unit, Department of Molecular Medicine and Surgery, and Center for Molecular Medicine, Karolinska Institutet, Karolinska University Hospital Solna, Stockholm, Sweden; <sup>c</sup>the Center for Pediatric Oncology and Hematology, Children's Hospital, Affiliate of Vilnius University Hospital Santariskiu Klinikos and <sup>d</sup>the Faculty of Medicine, Vilnius University, Vilnius, Lithuania; <sup>e</sup>the Center for Hematology and Regenerative Medicine (HERM), Department of Medicine, Huddinge, Karolinska Institutet, Stockholm, Sweden; <sup>f</sup>the Department of Human and Medical Genetics, Faculty of Medicine, Vilnius University, Vilnius, Lithuania; <sup>g</sup>the Department of Pediatrics, Institute of Clinical Sciences, Sahlgrenska Academy at University of Gothenburg, Gothenburg, Sweden; <sup>h</sup>the Center for Chronic Immunodeficiency and Center for Pediatrics, Medical Center - University of Freiburg, Faculty of Medicine and <sup>i</sup>the Faculty of Biology, University of Freiburg, Freiburg, Germany; <sup>j</sup>the Lithuanian University of Health Sciences (LUHS), Center of Pediatric Oncology and Hematology at Pediatric Department and Hospital of LUHS Kauno Klinikos and <sup>k</sup>the LUHS, Center of Chronic Respiratory Diseases in Children at Pediatric Department and Hospital of LUHS Kauno Klinikos, Kaunas, Lithuania; <sup>l</sup>the Department of Physiology, Biochemistry, Microbiology and Laboratory Medicine, Institute of Biomedical Sciences, Faculty of Medicine, Vilnius University and <sup>m</sup>the Centre of Laboratory Medicine, Vilnius University Hospital Santaros Klinikos, Vilnius, Lithuania; <sup>n</sup>the LUHS, Neurology Department and Hospital of LUHS Kauno Klinikos, Kaunas, Lithuania; <sup>o</sup>the Child Neurology Department at Children's Hospital, Affiliate of Vilnius University Hospital Santaros Klinikos, Vilnius, Lithuania; and <sup>p</sup>the Broegelmann Research Laboratory, Department of Clinical Sciences, University of Bergen, Bergen, Norway. E-mail: Bianca.Tesi@ki.se. Or: jelena.rascon@vuvl.lt.

\*Samuel C. C. Chiang is currently at the Division of Bone Marrow Transplantation and Immune Deficiency, Cincinnati Children's Hospital Medical Center, Cincinnati, Ohio, and Martha-Lena Müller is currently at Rudolf Virchow Center, University of Würzburg, Würzburg, Germany.

†Shared senior authorship.

This work was supported by a grant from the European Research Council (ERC) under the European Union's Seventh Framework Programme (grant no. FP/2007-2013; ERC grant agreement no. 311335), the Norwegian Research Council, the Swedish Foundation for Strategic Research, the Wallenberg Foundation, the Karolinska Institutet Center for Innovative Medicine (Y.T.B.), the Swedish Childhood Cancer Foundation (J.-I.H., Y.T.B., M.M.), as well as the Stockholm County Council, the Swedish Cancer Foundation, and the Swedish Research Council (J.-I.H., Y.T.B.), the Cancer and Allergy Foundation of Sweden (J.-I.H.), the German Ministry of Education and Research (grant no. BMBF 01EO1303), and the German Research Foundation (grant no. SFB1160, TP1; S.E.). B.T. is also supported by a doctoral student scholarship

from the Board of Postgraduate Studies at Karolinska Institutet. Computations were performed on resources provided by the Swedish National Infrastructure for Computing (SNIC) through the Uppsala Multidisciplinary Center for Advanced Computational Science under Project SNIC b2012204 and b2015280.

Disclosure of potential conflict of interest: S. Ehl reports a grant from Deutsche Forschungsgemeinschaft (grant no. SFB1160 TP4) and a grant from BMBF (grant no. BMBF 01EO1303) during the conduct of the study and grants from Union Chimique Belge outside the submitted work. J.-I. Henter reports grants from the Swedish Childhood Cancer Foundation, the Swedish Cancer Foundation, the Swedish Research Council, the Stockholm County Council, and the Cancer and Allergy Foundation of Sweden during the conduct of the study. M. Meeths reports grants from the Swedish Childhood Cancer Foundation during the conduct of the study. The rest of the authors declare that they have no relevant conflicts of interest.

## REFERENCES

1. Janka GE, Lehmborg K. Hemophagocytic syndromes—an update. *Blood Rev* 2014;28:135-42.
2. de Saint Basile G, Ménasché G, Fischer A. Molecular mechanisms of biogenesis and exocytosis of cytotoxic granules. *Nat Rev Immunol* 2010;10:568-79.
3. Meeths M, Bryceson YT, Rudd E, Zheng C, Wood SM, Ramme K, et al. Clinical presentation of Griscelli syndrome type 2 and spectrum of RAB27A mutations. *Pediatr Blood Cancer* 2010;54:563-72.
4. Brand H, Collins RL, Hanscom C, Rosenfeld JA, Pillalamarri V, Stone MR, et al. Paired-duplication signatures mark cryptic inversions and other complex structural variation. *Am J Hum Genet* 2015;97:170-6.
5. Netter P, Chan SK, Banerjee PP, Monaco-Shawver L, Noroski LM, Hanson IC, et al. A novel Rab27a mutation binds melanophilin, but not Munc13-4, causing immunodeficiency without albinism. *J Allergy Clin Immunol* 2016;138:599-601.e3.
6. Cetica V, Hackmann Y, Grieve S, Sieni E, Ciambotti B, Coniglio ML, et al. Patients with Griscelli syndrome and normal pigmentation identify RAB27A mutations that selectively disrupt MUNC13-4 binding. *J Allergy Clin Immunol* 2015;135:1310-8.e1.
7. The FANTOM Consortium and the RIKEN PMI and CLST (dgt). A promoter-level mammalian expression atlas. *Nature* 2014;507:462-70.
8. Vincent LM, Gilbert F, DiPace JJ, Ciccone C, Markello TC, Jeong A, et al. Novel 47.5-kb deletion in RAB27A results in severe Griscelli syndrome type 2. *Mol Genet Metab* 2010;101:62-5.
9. Zerah ML, DeWitt CA. Cutaneous findings in hemophagocytic lymphohistiocytosis. *Dermatology* 2015;230:234-43.

Available online March 6, 2018.  
<https://doi.org/10.1016/j.jaci.2018.02.031>

## Correlation of allergen-specific T follicular helper cell counts with specific IgE levels and efficacy of allergen immunotherapy



To the Editor:

Allergic rhinitis (AR) is caused by an IgE-mediated hypersensitivity reaction to airborne allergens. T<sub>H</sub>2 cells were long considered to regulate B-lymphocyte class-switch recombination to IgE by secreting the cytokines IL-4 or IL-13. However, recently, a novel CD4<sup>+</sup> T-cell subset, follicular helper T (T<sub>FH</sub>) cells, has been recognized as the central player in regulating B cells to support antibody response largely based on their localization in B-cell follicles and germinal centers.<sup>1</sup>

Mouse studies indicate that T<sub>FH</sub> cells, but not T<sub>H</sub>2 cells, regulate IgE production in patients with allergic asthma.<sup>1</sup> We demonstrated that nasal IL-4<sup>+</sup> T<sub>FH</sub> cell counts correlate to local IgE production in patients with eosinophilic nasal polyps.<sup>2</sup> Kamekura et al<sup>3</sup> reported a skewed T<sub>FH</sub> phenotype toward type 2 polarization in peripheral blood of patients with AR. However, exactly how allergen-specific T<sub>FH</sub> cells control the production of

## METHODS

### Genome-wide sequencing

Blood samples from the patients and, when available, their parents and siblings were obtained with informed consent according to the Declaration of Helsinki. The study was approved by the Regional Ethics Review Board in Stockholm, Sweden. DNA was isolated according to standard procedure. DNA from P1 and P2 was subjected to whole-genome sequencing with a TruSeq DNA PCR-free protocol followed by sequencing on an Illumina HiSeq X machine with an average coverage of 30×. Sequencing reads were analyzed with the pipeline SpeedSeq. In brief, reads were mapped to the human genome build GRCh37 with burrows-wheeler aligner, while calling of single nucleotide variants and structural variants was performed, respectively, with FreeBayes and Lumpy.<sup>E1</sup> The genomic region spanning *RAB27A* and *PIGB* was visualized with the Integrative Genomics Viewer.<sup>E2</sup> Integrative Genomics Viewer was also used to visualize discordant and split reads at the breakpoints. Split reads were mapped to the reference genome using the BLAT function of the University of California, Santa Cruz (UCSC) genome browser.

### Identification of structural variants breakpoints

To confirm the presence of the SV, primers were designed to PCR amplify the breakpoints of the mutant allele based on the information from discordant and split reads. PCR products were sequenced on an ABI3730 Genetic Analyzer. The breakpoint C-invE (Fig 2, B) was captured with the following primers: the forward 5'-CAACAGTTATGCGGCTCTCA-3' and the reverse 5'-TGCGTGCAGACTGGATAAAG-3'.

### Multiplex ligation-dependent probe amplification

To validate the presence of copy number alterations affecting *RAB27A* and *PIGB*, we used a custom-designed MLPA assay. MLPA probes were designed to cover the regions involved by the structural variants together with control probes to be used for normalization of the data. Probe sequences are listed in Table E2. The MLPA procedure was carried out according to the manufacturer's instructions (MRC-Holland, Amsterdam, The Netherlands). PCR products were separated on an ABI3500 XL Genetic Analyzer and analyzed with Peak Scanner 2.0 software.

### Immunological investigations

PBMCs from the families of P3 and P4, and healthy unrelated controls, were isolated within 24 hours of venipuncture and analyzed by flow cytometry for NK-cell and cytotoxic T-cell exocytosis at resting state and after 36 hours of 500U IL-2 stimulation (R&D Systems, Minneapolis, Minn) as previously described.<sup>E3</sup> NK-cell-mediated cytotoxicity was assessed via standard <sup>51</sup>Cr 4-hour assay, using labeled K562 cells as target, as previously described.<sup>E4</sup> FlowJo (v9.9, Treestar, Ashland, Ore) was used for flow cytometry and Prism (v7, Graphpad, La Jolla, Calif) for statistical analyses and plotting.

### Expression studies

Quantitative PCR was used to quantify *RAB27A* and *PIGB* transcript in PBMC-derived RNA from P3 and his parents, compared with unrelated healthy controls. Similarly, quantitative PCR was used to quantify transcripts in RNA isolated from melanocytes of healthy donors (n = 2). For *RAB27A*, one primer pair was designed to capture all isoforms, and another to capture only the isoform NM\_183235.2, disrupted by the SV. For *PIGB*, primer pairs were designed to target the mRNA before (upstream) and after (downstream) the breakpoint.

Publicly available FANTOM5 data were downloaded from <http://fantom.gsc.riken.jp/5/data/> (on June 26, 2017). The data set consists of cap analysis gene expression peaks for human samples in the form of relative log expression normalized data.<sup>E5</sup> Data for biological replicates (n = 3) were averaged. Further analysis and plotting was done in R version 3.3.1.

### Western blot of Rab27a

Cryopreserved PBMCs of patients (P3 and P4) and family members as well as local and transport controls were used to analyze Rab27a protein expression levels. To this end, freshly thawed cells were counted, sedimented, and resuspended in ice-cold lysis buffer (150 mM sodium chloride, 50 mM Tris, 2 mM EDTA, pH 7.6) supplemented with 1% (v/v) Triton X-100, 1% (v/v) Igepal CA-630 (Sigma-Aldrich, St Louis, Mo), and protease inhibitors (ThermoFisher, Waltham, Mass). Postnuclear lysates were separated by SDS-PAGE under reducing conditions (NuPage, ThermoFisher) and transferred to nitrocellulose membranes using the iBlot transfer system (ThermoFisher). Rabbit pAbs against Rab27a and Calnexin were purchased from ProteinTech Group and Enzo Life Science, respectively. For western blot performed on PBMCs from patient 5, the following antibodies were used: anti-RAB27A rabbit polyclonal antibodies #5415 and #5416, diluted 1:5000 (kind gift from Gillian Griffiths) and anti-beta-Actin mouse mAb, diluted 1:10,000 (Clone AC-15, Sigma Aldrich #A1978). Signals were visualized using ECL chemistry (ThermoFisher) and acquired using the Li-Cor Odyssey Fc system or the Fusion Imaging System (Vilber, Collégien, France).

## BRIEF CASE REPORTS

### Patient 1

P1, a girl of Lithuanian origins, presented at the age of 6 years with acute multiple vomiting episodes, headache, weakness, ataxia, and confusion. Cerebrospinal fluid analysis showed minimal pleocytosis and normal protein level. Brain magnetic resonance imaging (MRI) revealed multiple T2 hyperintensive lesions in cerebellum, periventricular regions, corpus callosum, and brain stem, prompting a diagnosis of acute disseminated encephalomyelitis (Fig E1, A). She subsequently experienced 8 relapses within the next 2 years managed with intravenous and oral steroids. During remissions she suffered from mild ataxia and tremor. At the age of 8 years, she was diagnosed with remitting-relapsing multiple sclerosis and started to receive preventive treatment with monthly intravenous immunoglobulin infusions for 18 months and achieved long-lasting remission. During follow-up, she underwent MRI investigations that demonstrated similar patterns, and in addition development of cerebellar atrophy. At age 13 years, following herpes simplex labialis infection, the patient presented with fever, jaundice, hepato- and splenomegaly, pancytopenia, hyperferritinemia, hypofibrinogenemia, and hypoalbuminemia, followed by ascites, pleural effusion, and encephalopathy. Liver enzymes were markedly elevated. Bone marrow biopsy showed no hemophagocytosis. Analysis of cytotoxic lymphocyte function showed defective cytotoxicity and exocytosis (Table E1). Neuroimaging showed nonspecific multifocal hyperintense white matter lesions in both hemispheres in FLAIR MRI (Fig 1, B). Nineteen days later the patient fulfilled the HLH diagnostic criteria (Table E1). Treatment according to HLH-2004 protocol was initiated but the patient's condition deteriorated and she died 48 days later because of massive central nervous system (CNS) lesions provoked by CNS infection (EBV reactivation and *Aspergillus fumigatus*). Her older brother died at the age of 1 year because of infectious mononucleosis. The patient displayed no signs of oculocutaneous albinism.

### Patient 2

P2, a boy of Swedish origin, was diagnosed with benign granuloma of the skin at the age of 2 years. At the age of 2.5 years he suffered from rapidly progressive sensorineuronal hearing

loss. At age 3 years, he developed fever, breathing difficulties with interstitial lung infiltrates, hepatosplenomegaly, increased liver enzymes, deteriorating motoric abilities, and low immunoglobulins. A primary EBV infection was detected. Recovery was obtained with antibiotic and antimycotic treatment, and immunoglobulin replacement. He suffered from recurrent episodes regarded as fungal pneumonias, although a fungal infection was never verified. At the age of 14.5 years, he deteriorated and was admitted to the hospital because of fever and coughing. An X-ray revealed interstitial lung disease. He also displayed splenomegaly, pericardial fluid, and elevated liver enzymes. One and a half week later he was again hospitalized with fever and low white blood cells. Spleen biopsy showed infiltration of histiocytic cells and *Aspergillus fumigatus*. A bone marrow examination did not show signs of malignancy and no or very little hemophagocytosis. He received antibiotics, antimycotics, and corticosteroids. At this point, fulfilling diagnostic criteria (Table E1), a diagnosis of HLH was established, and a secondary form of HLH was suspected. His condition deteriorated, with respiratory difficulties and increased inflammation. He received cyclosporin, antithymocyte globulin, and corticosteroids and later also etoposide. However, he continued to deteriorate and later died in the intensive care unit because of cardiac arrest. Genetic sequencing of *PRF1* was performed at the time without findings. One of his 3 sisters died at age 13 years because of an intracerebral tumor, later diagnosed as T-cell lymphoma (immunoblastic lymphoma). Another sister died at age 13 years in a clinical picture of interstitial pneumonia, aplastic anemia, aspergillus, liver disease, and progressive paresis. She also suffered from hearing loss. The third sister is healthy. The patient displayed no signs of oculocutaneous albinism.

### Patient 3

P3 is a second child of healthy nonconsanguineous parents of Lithuanian origin. At the age of 5 years, the boy was admitted because of acute ataxia, strabismus, diplopia, sleepiness, and papilledema. Three weeks earlier the patient had an episode of acute respiratory infection. There were multiple focal demyelinating lesions on brain MRI (Fig E1, B). He was diagnosed as having acute demyelinating encephalomyelitis, and intravenous methylprednisolone pulse markedly improved symptoms. Eight months later he was admitted to the intensive care unit because of acute respiratory failure, fever, and reappearance of previously observed neurological symptoms. He also had a maculopapular rash. Skin biopsy showed granulomatous dermatitis, CD3/CD4- and CD3/CD8-positive cells, and CD68-positive histiocytes (Fig 1, C). Lung computed tomography showed focal confluent infiltration and enlarged mediastinal lymph nodes (1-1.3 cm; Fig E1, C). A lung biopsy showed focal lymphocyte and macrophage infiltration (predominance of CD3 T lymphocytes, 20% CD20-positive cells, CD68 macrophages). Slightly decreased immunoglobulin G subtypes were found, but routine test results for cellular immunity were normal. The patient became steroid-dependent for the subsequent 3 years, after which, at the age of 9 years, following tonsillitis, he developed persistent fever with elevated liver enzymes, hepatomegaly, neutropenia, and anemia. Analysis of cytotoxic lymphocyte function showed defective

cytotoxicity and exocytosis (Fig 1, D-F). A diagnosis of HLH was established (Table E1) and treatment according to HLH-2004 protocol was initiated. At the age of 10 years, P3 received a hematopoietic stem cell transplantation (HSCT) from his HLA-identical brother. A reduced intensity conditioning based on fludarabine (180 mg/m<sup>2</sup>) and melphalan (140 mg/m<sup>2</sup>) was used. For graft-versus-host disease (GvHD) prophylaxis, cyclosporine A and mycophenolate mofetil were used. The patient developed an acute GvHD grade II (skin +++, GI +), which later developed into a chronic form with skin involvement that has resolved. The patient displayed no signs of oculocutaneous albinism (Fig E1, D).

### Patient 4

P4 is the second child of healthy nonconsanguineous parents from Lithuania. P4 developed skin granulomas at the age of 16 months. At the age of 1 year 9 months, she developed ataxia, impaired walking, and tremor after varicella infection. The symptoms improved following a course of prednisone, but subsequent similar attacks followed. In 2 exacerbation episodes EBV reactivation was detected. MRI showed numerous demyelinating foci in the cerebellum, and a massive confluent conglomerate in the splenium involving both hemispheres and the spinal cord. At the age of 7 years 8 months, the biopsy of CNS lesions was performed showing nonmalignant reactive lymphoid infiltrates (CD3<sup>+</sup>, CD4<sup>+</sup>, CD8<sup>+</sup>, GranB<sup>+</sup>, CD30<sup>-</sup>), nonspecific granulomatous microfoci. No signs characteristic of HLH were detected (Table E1). Analysis of cytotoxic lymphocyte function showed defective cytotoxicity and exocytosis (Fig 1, G-I). At the age of 8 years, P4 received an HSCT from a matched unrelated donor. A reduced-intensity conditioning based on fludarabine (150 mg/m<sup>2</sup>) and treosulphan (42 g/m<sup>2</sup>) was used. For GvHD prophylaxis, alemtuzumab (0.6 mg/kg), cyclosporine A, and mycophenolate mofetil were used. At the time of report, the patient is 2 months after HSCT. The patient displayed no signs of oculocutaneous albinism.

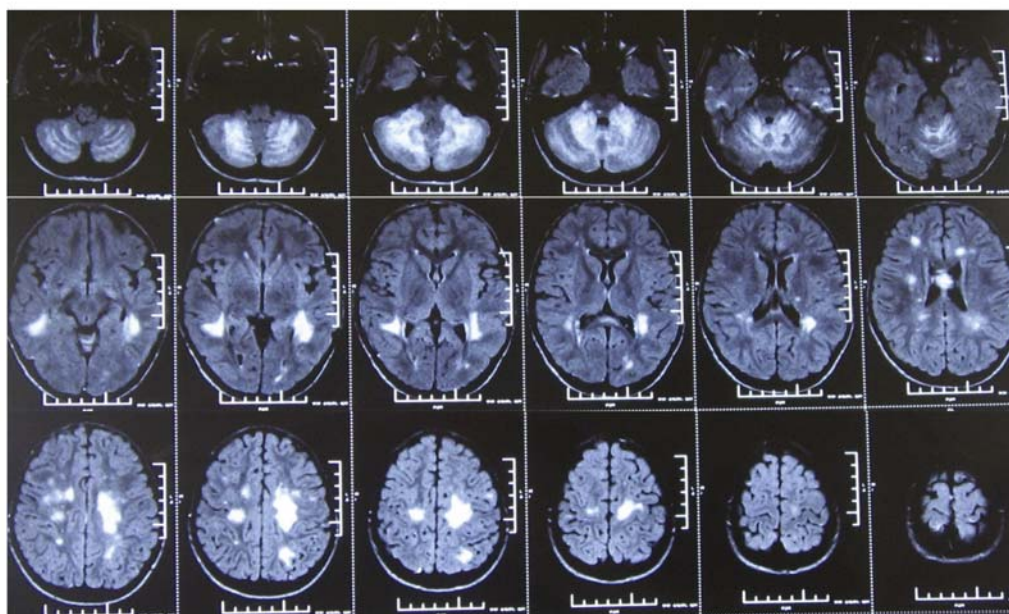
### Patient 5

P5 is a 14-year-old boy from Russia. He had uncomplicated infectious mononucleosis at age 2 years without signs of HLH and good clinical recovery. At the age of 10 years, he developed recurrent fever flares lasting up to 3 weeks without obvious trigger. The overall condition was not significantly impaired. There were no significant cytopenias and the patient never met diagnostic criteria for HLH. At the age of 11.3 years, the patient rapidly developed splenomegaly with pancytopenia. Splenectomy corrected the cytopenia and diminished the frequency and intensity of fever flares. Enlargement of abdominal lymph nodes was noted and a biopsy showed only follicular hyperplasia. At the age of 12.8 years, he had sudden onset of cervical lymphadenopathy and was diagnosed with Hodgkin lymphoma, stage IVA. He responded well to treatment according to the GPOH-HD 2002 protocol and is currently in full remission. The combination of recurrent fever flares, splenomegaly, and lymphoma prompted further immunological investigations. NK-cell and cytotoxic T lymphocytes cytotoxicity and exocytosis were defective (Table E1). The patient displayed no signs of oculocutaneous albinism.

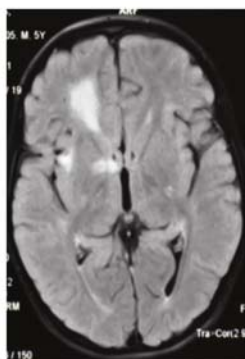
## REFERENCES

- E1. Chiang C, Layer RM, Faust GG, Lindberg MR, Rose DB, Garrison EP, et al. SpeedSeq: ultra-fast personal genome analysis and interpretation. *Nat Methods* 2015;12:966-8.
- E2. Thorvaldsdóttir H, Robinson JT, Mesirov JP. Integrative Genomics Viewer (IGV): high-performance genomics data visualization and exploration. *Brief Bioinform* 2013;14:178-92.
- E3. Chiang SCC, Theorell J, Entesarian M, Meeths M, Mastafa M, Al-Herz W, et al. Comparison of primary human cytotoxic T-cell and natural killer cell responses reveal similar molecular requirements for lytic granule exocytosis but differences in cytokine production. *Blood* 2013;121:1345-56.
- E4. Meeths M, Chiang SCC, Wood SM, Entesarian M, Schlums H, Bang B, et al. Familial hemophagocytic lymphohistiocytosis type 3 (FHL3) caused by deep intronic mutation and inversion in *UNC13D*. *Blood* 2011;118:5783-93.
- E5. The FANTOM Consortium and the RIKEN PMI and Clst (dgt). A promoter-level mammalian expression atlas. *Nature* 2014;507:462-70.

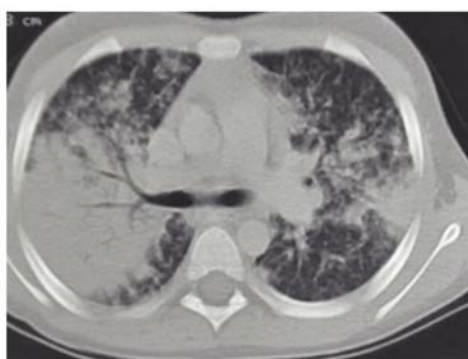
**A** Patient P1



**B** Patient P3



**C** Patient P3



**D** Patient P3



**FIG E1.** **A**, Brain MRI of P1 at onset of disease, axial series. **B**, Brain MRI of P3 at onset of disease. **C**, Lung computed tomography scan of P3. **D**, Photo of P3 showing normally pigmented hair.

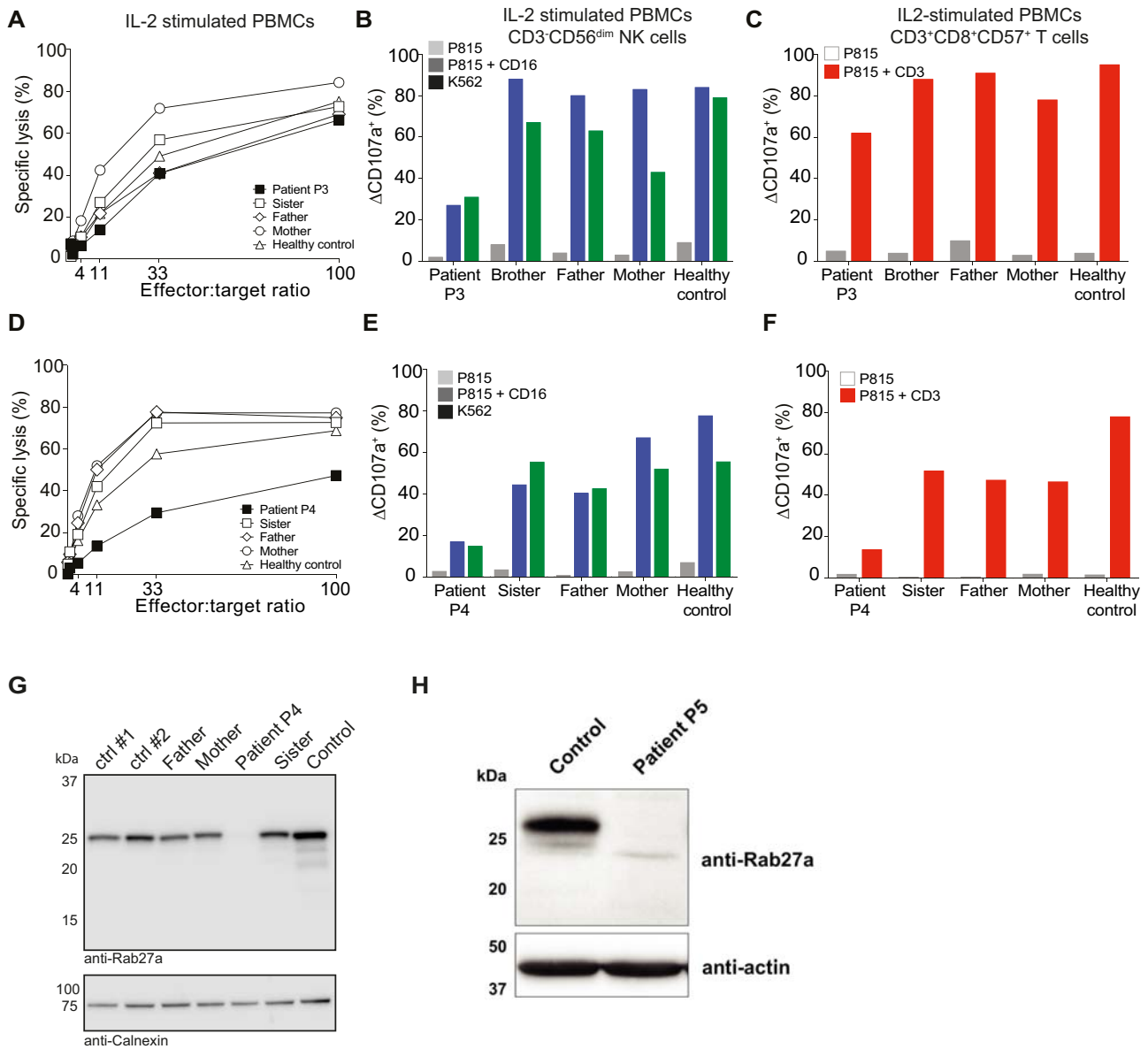


**FIG E2.** **A**, NK-cell cytotoxicity assay in IL-2-stimulated PBMCs from P3 and relatives. **B**, NK-cell degranulation assay in IL-2-stimulated PBMCs from P3 and relatives. **C**, CD8<sup>+</sup>CD57<sup>+</sup> T-cell degranulation assay in IL-2-stimulated PBMCs from P3 and relatives. **D**, NK-cell cytotoxicity assay in IL-2-stimulated PBMCs from P4 and relatives. **E**, NK-cell degranulation assay in IL-2-stimulated PBMCs from P4 and relatives. **F**, CD8<sup>+</sup>CD57<sup>+</sup> T-cell degranulation assay in IL-2-stimulated PBMCs from P4 and relatives. **G**, Western blot analysis of Rab27a in P4 and relatives. **H**, Western blot analysis of Rab27a in P5.

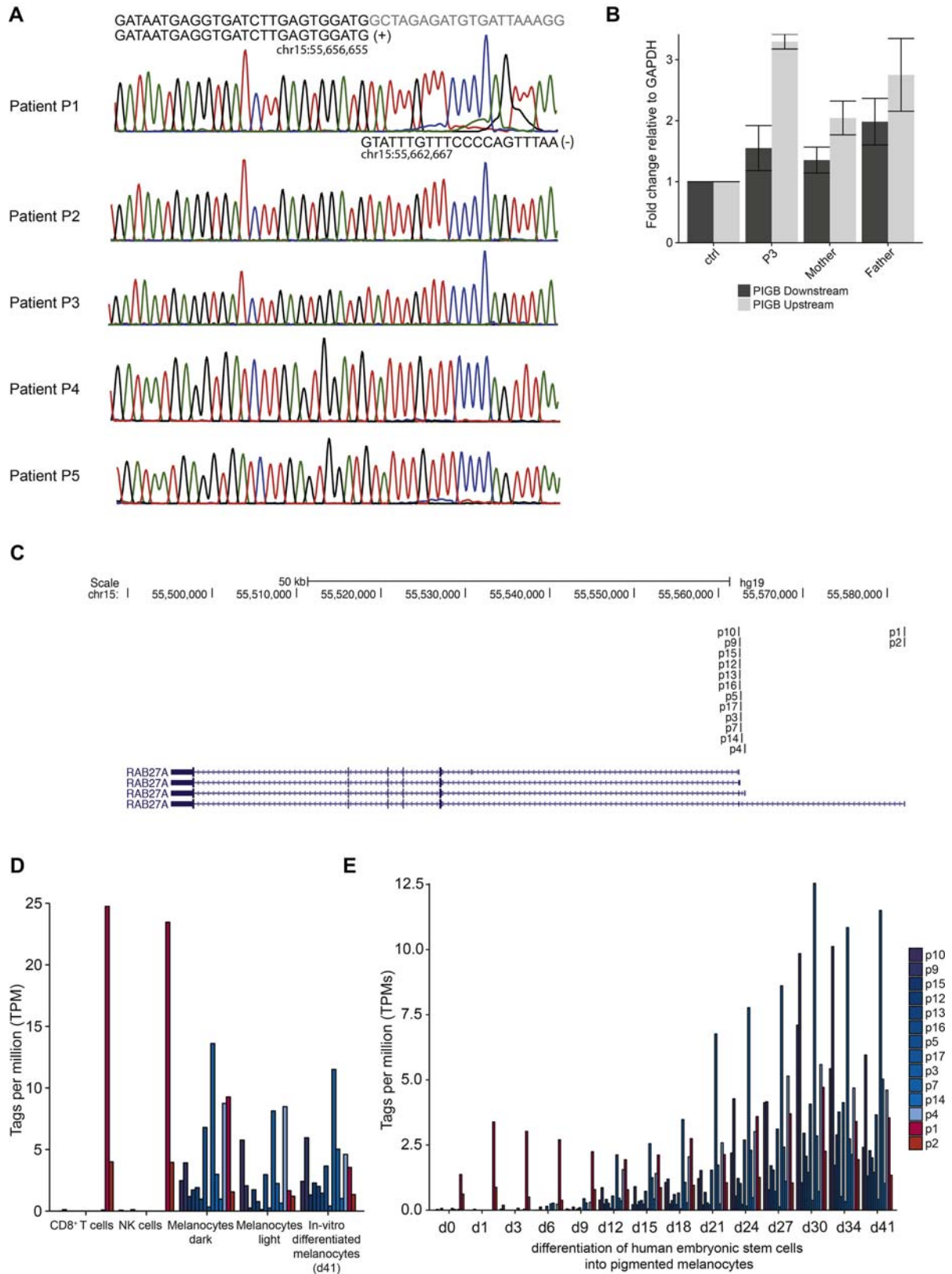


**FIG E3.** **A**, Sanger trace for breakpoint C-inV in all patients. **B**, Quantitative PCR of *PIGB* to quantify RNA from PBMCs isolated in P3 and relatives. **C**, UCSC Genome browser screenshot showing localization of the *RAB27A* TSS according to FANTOM5 CAGE data from human cells. p1 is the TSS for the isoform NM\_183235.2. **D**, Tags per million at the different *RAB27A* TSS from the FANTOM5 CAGE data. **E**, Tags per million at the different *RAB27A* TSS during differentiation of human embryonic stem cells into pigmented melanocytes (d, day). *CAGE*, Cap analysis gene expression.

**TABLE E1.** Clinical and laboratory findings at diagnosis of HLH

Family	1	2	3	4	5
Patient	P1	P2	P3	P4	P5
Ethnic origin	Lithuania	Sweden	Lithuania	Lithuania	Russia
Familial disease	Yes	Yes	No	No	No
Parental consanguinity	No	No	No	No	No
Sex	Female	Male	Male	Female	Male
<i>RAB27A</i> allele 1	Deletion, c.559C>T (p.Arg187Trp)	Dup-Inv	Dup-Inv	Dup-Inv	Dup-Inv
<i>RAB27A</i> allele 2	Dup-Inv	c.239G>C (p.Arg80Thr)	Dup-Inv	Dup-Inv	c.550C>T (p.Arg184*)
Age at diagnosis of HLH (y)	14	14.5	9	No HLH	No HLH
Fever	Yes	Yes	Yes	No	Yes (intermittent)
Splenomegaly	Yes	Yes	No	No	Yes, chronic (splenectomized)
Hepatomegaly	Yes	Yes	Yes	No	Transient, self-limiting
Hemoglobin (g/L)	83	87	90	Within normal	ND
Neutrophils ( $10^9/L$ )	0.45	0.80	0.14	Within normal	ND
Platelets ( $10^9/L$ )	35	54	194	Within normal	ND
Triglycerides (mmol/L)	2.49	5.8	2.71	Within normal	ND
Fibrinogen (g/L)	0.6	0.4	0.6	1.51	ND
Hemophagocytosis	No	No	Yes	ND	ND
Ferritin ( $\mu\text{g/L}$ )	2451	49000	12000	Within normal	ND
Soluble CD25 (pg/mL)	20512.4	ND	16437	1760	ND
NK-cell activity	ND	ND	Defective	Defective	Defective
NK-cell degranulation	Defective, 3.1% $\Delta\text{CD107a}$	ND	Defective, 6% $\Delta\text{CD107a}$	Defective, 3.3% $\Delta\text{CD107a}$	Defective, 0.6% $\Delta\text{CD107a}$
Neurological manifestations	Yes, before HLH onset	Yes	Yes, before HLH onset	Yes	No
Pathological CSF	Yes	ND	Yes	Yes	ND
Treatment active disease	HLH-2004	Cortico, CSA, ATG	HLH-2004	Cortico, MMF	
Remission at 2 mo	No	No	Yes	NA	
Age at HSCT	Not done		10	7	
Outcome and follow-up	Deceased 48 d after HLH onset		Alive 19 mo after HSCT	Alive at 7 y	Alive at 16 y
Other manifestations	No	Skin granuloma, lung infiltrates	Skin granuloma, lung infiltrates	Skin granuloma, isolated CNS involvement	Hodgkin lymphoma at 13 y, recurrent fever episodes from 10 y

ATG, Antithymocyte globulin; Cortico, corticosteroids; CSA, cyclosporine A; CSF, cerebrospinal fluid; Dup-Inv, Duplication-Inversion; MMF, mycophenolate mofetil; NA, not applicable/available; ND, no data.

**TABLE E2.** MLPA probes

Gene	Size (bp)	Used for <a href="#">Figure 2, C</a>
GABRA4_fam-pilot	84	Control probe
RAB27A_probe5	87	Probe C in <a href="#">Figure 2, C</a>
RAB27A_probe6	90	
RAB27A_probe7	93	
RAB27A_probe8	96	Probe D in <a href="#">Figure 2, C</a>
RAB27A_probe4	99	Probe B in <a href="#">Figure 2, C</a>
RAB27A_probe3	102	
Stern PCLN13q	105	Control probe
RAB27A_probe10	108	Probe E in <a href="#">Figure 2, C</a>
RAB27A_probe9	111	
RAB27A_probe1	114	Probe A in <a href="#">Figure 2, C</a>
PIGB_probe11	117	Probe F in <a href="#">Figure 2, C</a>
RB1ex23	129	Control probe
MRPL41_e1_132	132	Control probe
SRY	135	Control probe
GABRA4_fam-pilot_A	gggttcctaagggttgaCAGCCTGTTGTCATAACCATCG	
GABRA4_fam-pilot_B	/5Phos/AGCAAAGCTGCCAGGATGCGtctagattggatcttctggcac	
Stern PCLN13q_A	gggttcctaagggttgaGACACAAGGGTGAAAAATGCACG	
Stern PCLN13q_B	/5Phos/TTTCAGGGTGTGTTTGCATATGATTTAATCAATCAGTATGtctagattggatcttctggcac	
RB1ex23_A	gggttcctaagggttgaGTCACCAATACCTCACATTCCTCGAAGCCCTTACAAGTTTCCT	
RB1ex23_B	/5Phos/AGTTCACCCCTACGGATTCCCTGGAGGGAACATCTATATTTACCTctagattggatcttctggcac	
MRPL41_e1_132_A	gggttcctaagggttgaGACCCTGACAACCTGGAAAAGTACGGCTTCGAGCCACACAGGAG	
MRPL41_e1_132_B	/5Phos/GGAAAGCTCTTCCAGCTCTACCCAGGAAGCTTCCTGCGCTAGCTGtctagattggatcttctggcac	
SRY_A	gggttcctaagggttgaCAGTGCAAAGGAAGGAAGAGCTTCTCCGGAGAGCGGGAATATTCT	
SRY_B	/5Phos/CTTGCACAGCTGGACTGTAATCATCGCTGTTGAATACGCTTAACATAGtctagattggatcttctggcac	
RAB27A_p5_A	gggttcctaagggttgaGGACTTCAGGAAGCTGCAATGTTT	
RAB27A_p5_B	/5Phos/GCTTTTGTGAATTTCTTCCCtctagattggatcttctggcac	
RAB27A_p6_A	gggttcctaagggttgaCACAGAACCTCAGAGAAGCCTTGA	
RAB27A_p6_B	/5Phos/GGGGCAACTGGTCAACCAATTAGTctagattggatcttctggcac	
RAB27A_p7_A	gggttcctaagggttgaCAGACCTCGTGGTCCCCTCAGA	
RAB27A_p7_B	/5Phos/GGCAGCCAGTTCATCCCTCTCAGTGGtctagattggatcttctggcac	
RAB27A_p8_A	gggttcctaagggttgaGCCTTCTAAGCCGTCTCGCTGACTTGT	
RAB27A_p8_B	/5Phos/GTCTACCTCCACCGCAAATCCAGCTGtctagattggatcttctggcac	
RAB27A_p4_A	gggttcctaagggttgaGATCCAAGTCTCCCTTCAAGAAGTT	
RAB27A_p4_B	/5Phos/GGTAATTAGGGTGAGGTGGAATGATGTACTctagattggatcttctggcac	
RAB27A_p3_A	gggttcctaagggttgaCAACTGGCCAGCTGTCACTCAAATGCTAATT	
RAB27A_p3_B	/5Phos/GTGTCTATCATCTGCTTTCTCTAATAGCCtctagattggatcttctggcac	
RAB27A_p10_A	gggttcctaagggttgaGTGGCAAGATGGGTGGTAAGTCCATAAATACTTTA	
RAB27A_p10_B	/5Phos/GAAGCTGTATGCCAGTTATTTTCGTTCCATGtctagattggatcttctggcac	
RAB27A_p9_A	gggttcctaagggttgaGCTTTAAGAATGGTGTGGAGGGACCAGAGGTCACTA	
RAB27A_p9_B	/5Phos/CTGTGCCTTACAAGGAGCCAACCAGAGCAGCAGtctagattggatcttctggcac	
RAB27A_p1_A	gggttcctaagggttgaGAGGCATGACCATTTGATCGCACCACTCCTTCAGGAAT	
RAB27A_p1_B	/5Phos/CCAGACTTGTCCACACACCGTTCCATTTCGCTTctagattggatcttctggcac	
PIGB_p_11_A	gggttcctaagggttgaGAGGACATTTATGTTTCCGGAACAGAATACCAATGCTA	
PIGB_p_11_B	/5Phos/CAGAATGTTGAGTCCCCTACTGACCTACTTCCCTctagattggatcttctggcac	